

Design and Experimental Study of a Compliant Feet Quadruped Robot with Closed-Chain Mechanism Legs

Zhirong Wang, Erbao Dong*, Member, IEEE, Hao Wang, Chunshan Liu, Guowei Ma, Min Xu, Jie Yang

Abstract— The locomotion performances of a quadruped robot with compliant feet based on closed-chain mechanism legs are presented. The legs of this quadruped robot were made up of six-bar linkage mechanism with one degree of freedom. And a special foot trajectory could be gained through kinematic analysis and optimum design of the six-bar linkage mechanism. In order to reduce the impact force of quadruped robot's walking on the ground, two semicircle feet with different thickness were designed as compliant feet. The experimental results of this quadruped robot with different stiffness feet showed that the semicircle feet could reduce the driving torque and current of motors. This primary investigation illustrated that the compliant feet could improve the locomotion performance of a quadruped robot based on closed-chain mechanism legs.

I. INTRODUCTION

To develop the multi-legged robot with high locomotion velocity and high energy efficiency is always one of the most important issues in robotics research field. Many excellent multi-legged robot have been developed, which were based on the open-chain mechanism and closed-chain mechanism legs.

In open-chain series mechanism leg, each joint is driven by an actuator directly, to offer high motion flexibility for the multi-legged robot. Mostly existed multi-legged robots used open-chain mechanism legs. Each leg joint of the *LittleDog* [1, 2] and the *Scorpion* [3] was actuated by the swing output of the motor fixed on the joint directly. These two robots had good ability to crawl over rough obstacle. Inspired by the animal's leg locomotion, the linear actuation was used to drive each joint of the open-chain mechanism legs in some robot, such as the *BISAM* [4, 5], *BigDog* [6], and *HyQ* [7, 8]. Each joint of the *BISAM* was driven by the motor with a linear screw system and the driving system of the *BigDog* and *HyQ*'s were linear hydraulic system. The *BigDog* had a high stability and could walk and trot on slope, ice ground and other rough terrains.

However, the open-chain mechanism may result in low efficiency and limit the rapid leg locomotion of multi-legged

Resrach is supported by National Natural Science Foundation of China (No. 51275501, 51105349) and the Fundamental Research Funds for the Central Universities.

Zhirong Wang, Erbao Dong*, Hao Wang, Chunshan Liu, Guowei Ma, Min Xu, Jie Yang are with the Department of Precision Machinery and Precision Instrumentation, University of Science and Technology of China, Hefei, Anhui Province, 230026, China (*corresponding author to provide phone: 086-551-63601482 ; e-mail: ebdong@ustc.edu.cn).

robot, due to the actuators' swing reciprocation motion.

Therefore, the crank-rocker closed-chain mechanism was used to design the multi-legged robot by some researcher, in order to obtain a high efficiency. Jansen's *strandbeest* [9] was a multi-legged robot and could walk steady on the beech only driven by the wind. The leg of this robot was made up of eight-bar crank-rocker linkage. *Waterrunner* was a lizard-like quadruped robot with four-bar crank-rocker mechanism legs, and it could run rapidly on the water using the drag force [10, 11].

Whereas, there is not motion flexibility in the close-chain mechanism leg, due to its one degree of freedom. A multi-legged robot based on the hybrid-driven mechanism in [12] was built to solve this problem. The hybrid-driven mechanism is a crank-rocker mechanisms in which there are servo actuators to adjust the foot trajectory.

Besides, the driving torque in the crank-rocker mechanism is uneven in a cycle, which is unfavorable for locomotion of legged robot based on closed-chain mechanism. Adding complaint mechanism into the closed-chain mechanism leg may be a mean to reduce the driving torque, like the compliant tissue's storing energy in animal leg locomotion. In [13], Alexander illustrated that the compliant segment near the foot had a biggest benefit in energy storing through bionic study.

Wherefore, in this paper, the locomotion performance of a kind of compliant foot in the multi-legged robot based on closed-chain mechanism legs was studied, based on the existed platform. The kinematic analysis on the applied closed-chain mechanism leg will be given in Section II. And then, the mechanical design and the compliant foot test will be introduced in Section III. Section IV will give the experimental results of the robot based on closed-chain mechanism with compliant feet. Finally, the Conclusion and Future work will be discussed.

II. MECHANISM ANALYSIS

A. Closed-chain Mechanism Leg

As shown in Fig.1, the closed-chain mechanism leg used in our legged robot is a six-bar crank-rocker linkage mechanism. The crank of the mechanism is the *a-bar* driven by a constant speed in the leg locomotion; *b-bar* and *e-bar* are the leg's frame fixed to the body of robot; *g-bar* and *k-bar* are the shank, and the foot is fixed on the lower end of *k-bar*.

The six-bar linkage mechanism was a compromise between

four-bar and eight-bar. The mechanism complexity of six-bar crank-rocker linkage system is less than eight-bar linkage. While, the number of six-bar's parameters to optimize the foot trajectory is more than the four-bar. The *l-bar* (in dash line) is a linear rigid foot of the linkage mechanism leg, and the foot trajectory could be obtained by the lower end of the *l-bar*. The effect of the angle between the *k-bar* and *l-bar* is to increase stand phase time.

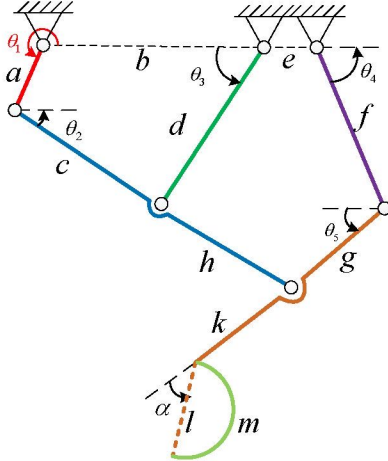


Fig. 1. Close-chain mechanism leg with compliant foot. The *a-bar* is the crank of the closed-chain mechanism; *l-bar* is a rigid foot; *m-bar* is a semicircle compliant foot. The θ_1 is the Laplace parameter to represent the angular position of the crank, and θ_2 , θ_3 , θ_4 and θ_5 are associated parameters to represent the angle between the level and different bars.

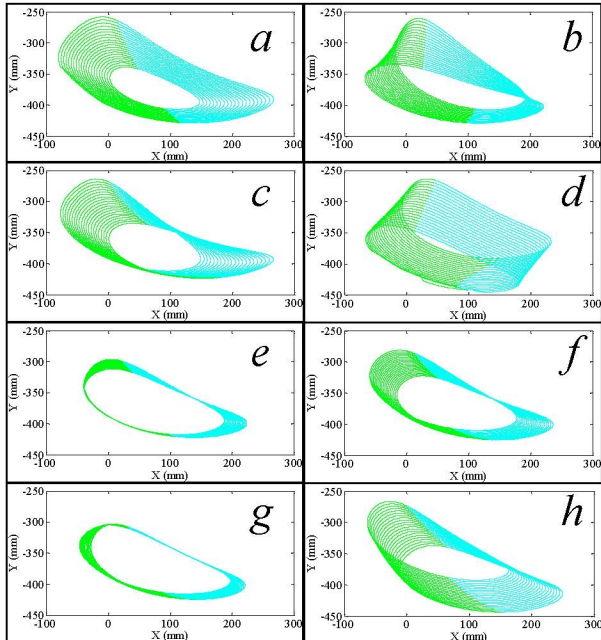


Fig.2. Foot trajectory variations by the dimension change of different bars. (From *a-bar* to *h-bar*)

The influence of different bars on the foot trajectory is shown in Fig. 2. With the same length change, different bars have different influence on the parameters of the foot trajectory: the change of the *a-bar*'s length mainly affects the size of workspace; *b-bar* mainly influences the left half trajectory, where the step height changes slightly; when length of *c-bar* or the *h-bar* changes, the horizon position and pitch

angle of the trajectory would change, also the height of left half trajectory changes; the *d-bar* mainly influences the vertical position of the trajectory; the *e-bar* and *g-bar* have fine-tuning on the foot trajectory; when the *f-bar* length changes, the stand phase time would change.

After an optimization, a special trajectory was obtained, and related dimensions are listed in TABLE I.

TABLE I
DIMENSIONS OF MECHANISM

Length of bars (mm)					Angle (degrees)
<i>a</i>	<i>b</i>	<i>c</i>	<i>d</i>	<i>e</i>	<i>a</i>
50	150	140	140	30	35
<i>f</i>	<i>g</i>	<i>h</i>	<i>k</i>	<i>l</i>	
170	120	140	71	105	

There are many existed compliant legs in those legged robots based on open-chain mechanism, such as Telescopic/prismatic leg in BigDog [6], bow leg in hopping robot [14] and C-leg in RHex [15, 16]. In this paper, a semicircle foot, which is like the C-leg and withstand the impact force in chord direction like a linear spring, would be adapted as the compliant foot, considering the existed legged robot based on closed-chain mechanism. The *m-bar* in Fig. 1 is the semicircle foot, and its diameter equal to the length of the *l-bar*.

B. Kinematic Analysis

There are two close loops in this six-bar mechanism. The constraint of first close-loop *a-b-d-c* can be described as

$$\begin{cases} a \cos \theta_1 + c \cos \theta_2 + d \cos \theta_3 = b \\ a \sin \theta_1 - c \sin \theta_2 + d \sin \theta_3 = 0 \end{cases} \quad (1)$$

Solving Eq. (1), yields, θ_2 and θ_3 ,

$$\begin{cases} \theta_2 = 2 \tan^{-1} \left(\frac{X_2 + \sqrt{X_2^2 + Y_2^2 - Z_2^2}}{Y_2 + Z_2} \right) \\ \theta_3 = 2 \tan^{-1} \left(\frac{X_3 + \sqrt{X_3^2 + Y_3^2 - Z_3^2}}{Y_3 + Z_3} \right) \end{cases} \quad (2)$$

where

$$X_2 = 2ac \sin \theta_1, \quad Y_2 = 2bc - 2ac \cos \theta_1$$

$$Z_2 = a^2 + b^2 + c^2 - d^2 - 2ab \cos \theta_1$$

$$X_3 = 2ad \sin \theta_1, \quad Y_3 = 2bd - 2ad \cos \theta_1$$

$$Z_3 = a^2 + b^2 + d^2 - c^2 - 2ab \cos \theta_1$$

The constraint of the second close-loop *d-h-g-f-e* can be described as

$$\begin{cases} -d \cos \theta_3 + h \cos \theta_2 + g \cos \theta_5 - f \cos \theta_4 = e \\ -d \sin \theta_3 - h \sin \theta_2 + g \sin \theta_5 + f \sin \theta_4 = 0 \end{cases} \quad (3)$$

Solving Eq. (3), yields, θ_4 and θ_5 ,

$$\begin{cases} \theta_4 = 2 \tan^{-1} \left(\frac{X_4 - \sqrt{X_4^2 + Y_4^2 - Z_4^2}}{Y_4 + Z_4} \right) \\ \theta_5 = 2 \tan^{-1} \left(\frac{X_5 - \sqrt{X_5^2 + Y_5^2 - Z_5^2}}{Y_5 + Z_5} \right) \end{cases} \quad (4)$$

where

$$\begin{aligned}
X_4 &= 2(d \sin \theta_3 + h \sin \theta_2) f \\
Y_4 &= 2(-e - d \cos \theta_3 + h \cos \theta_2) f \\
Z_4 &= d^2 + h^2 + e^2 + f^2 - g^2 \\
&\quad - 2dh \cos(\theta_2 + \theta_3) + 2e(d \cos \theta_3 - h \cos \theta_2) \\
X_5 &= 2(d \sin \theta_3 + h \sin \theta_2) g \\
Y_5 &= 2(e + d \cos \theta_3 - h \cos \theta_2) g \\
Z_5 &= d^2 + h^2 + e^2 + g^2 - f^2 \\
&\quad - 2dh \cos(\theta_2 + \theta_3) + 2e(d \cos \theta_3 - h \cos \theta_2)
\end{aligned}$$

Defining that the rotary center of the crank is the origin of coordinate, the ground touch point's coordinate of semicircle foot can be expressed as

$$\begin{cases} x = b + e + f \cos \theta_4 - (g + k) \cos \theta_5 - r \cos(\theta_5 + \alpha) \\ y = -f \sin \theta_4 - (g + k) \sin \theta_5 - r \sin(\theta_5 + \alpha) \end{cases} \quad (5)$$

where r is the radius of the semicircle foot.

Thus, with the mechanism dimensions in TABLE I, the trajectory of semicircle foot's ground touch point is shown in Fig.3. The angle numbers show degrees of the crank angle at the related blue point.

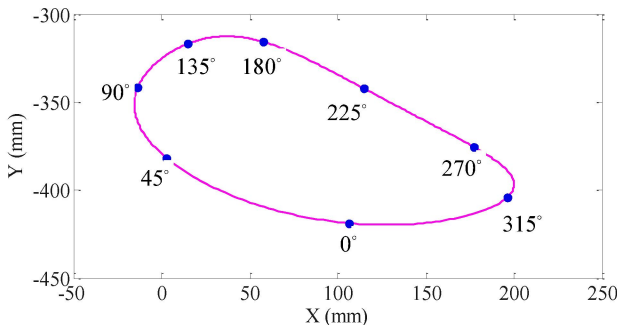


Fig. 3. The trajectory of semicircle foot's the ground-touch point. The angle numbers are degrees of crank angle related to the blue points.

III. MECHANICAL DESIGN

A. Quadruped robot based on closed-chain mechanism.

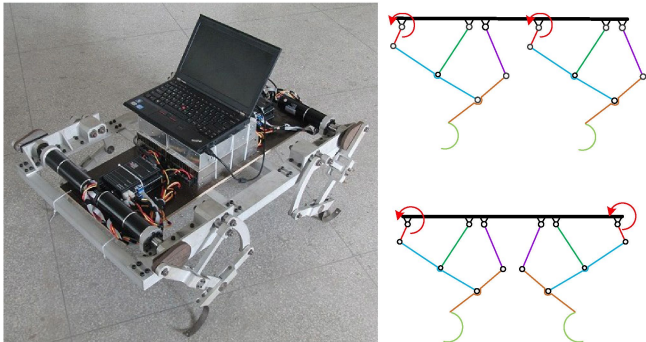


Fig. 4. Legged robot based on closed-chain mechanism and compliant feet. The left is a photograph of quadruped robot prototype; the upper right is the configuration that both elbow joints angled in parallel in side view, and bottom right is the configuration that both elbow joints angled inwards in side view.

Based on above mechanism analysis, a quadruped robot with closed-chain mechanism leg was built and shown in Fig.

4. Four legs were designed in modular with the same closed-chain mechanism, so that the robot could have different configurations: inner trigger, parallel trigger. Each leg was driven by a DC motor and the mechanism data could be achieved from the motor encoder without any other angle sensors. The current, speed data could be also achieved from the EPOS2 Controller connecting the motor.

B. Semicircle foot and their stiffness

As shown in Fig. 5, the semicircle foot was designed by 210 degrees, 15 degrees extension on each side. There are two holes in the diameter direction for fixing, at the point of 15 degrees and 195 degrees. For similarly consideration, the diameter of the foot is 105 mm, same to the length of the *l-bar*, and the width is 20 mm, same to the rigid foot. For comparison consideration, two semicircle feet with different thickness, 2 mm and 2.5mm, were designed after structural analysis.

For preliminary consideration, the stiffness of the semicircle feet will be modeled as linear spring, and its stiffness was measured in the diameter direction.

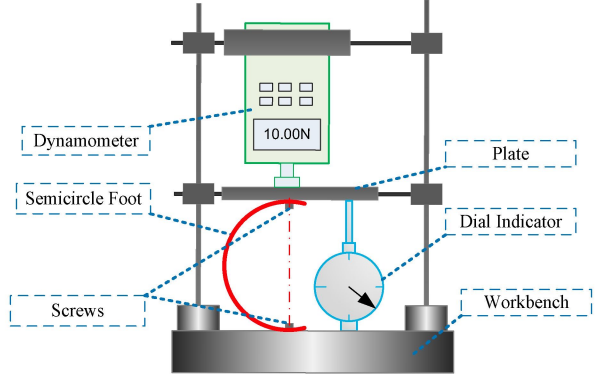


Fig. 5. Equipment for measuring stiffness of semicircle feet. Semicircle foot and dial indicator are all between the workbench and plate.

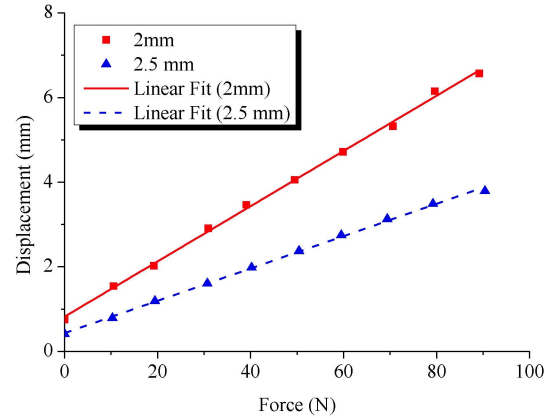


Fig. 6. The stiffness of the semicircle feet measured in diameter direction. The horizontal coordinate is the push force to the feet, and the vertical coordinate is the displacement of the dial indicator. The points in red square and blue triangle are the measured data, and the red solid line and blue dash line are the linear fitting results of the measured data.

Shown in Fig.5, a dynamometer with an accuracy of 0.01N was used to measure the force of the semicircle foot standing against in diameter direction, and a dial indicator was used to measure the displacement of the foot in diameter direction. The semicircle foot was fixed to the workbench and plate with

screws through the two holes in diameter direction, which could commit that the push force is always in diameter direction. The two side of the dial indicator were in contact with workbench and the plate, respectively. When the dynamometer offer a push force to the plate, the semicircle foot is compressed in diameter direction and the dial indicator presents the displacement. For each semicircle foot, ten groups of data, the forces varying from 0 N to 90 N and related displacements, were measured and shown in the Fig. 6.

As the stiffness of the semicircle in diameter direction is approximately constant, linear fittings of the measured data were carried out, and the relationship between the displacement (D) and force (F) is expressed in $D = a + b * F$. The parameters of linear fitting are presented in TABLE II.

TABLE II
LINEAR FITTING PARAMETERS

2 mm		2.5 mm	
value	Standard error	value	Standard error
a	0.822	0.432	0.027
b	0.065	0.001	0.038
			0.001

From the TABLE II, the stiffness of the two thicknesses of semicircle feet could be calculated. For the displacement in the figure is only the indicate number of dial indicator, so the parameter “ a ” is need not be in consideration in the stiffness calculating, and the stiffness is the reciprocal of the parameter “ b ”. Thus, the stiffness of the 2 mm thickness foot is 15.38 N/mm, and the stiffness of 2.5 mm thickness is 26.32 N/mm.

IV. EXPERIMENTS

Two experiments in inner trigger and parallel trigger configurations respectively, were conducted on the ground to test the performances of the compliant feet. The motor current was measured to evaluate the driving torque, as the relationship between the motor current and driving torque is linear. In the experiments, the actual current was measured per 50 ms, with a condition that the crank was driven by a clockwise speed of 12 rpm.

A. Robot in configuration that both elbow joints angled inwards

When the robot walk in inner trigger configuration, it is symmetrical in forward direction, and the feet trajectories of front and back legs were different. The front legs used the forward foot trajectory, while the back legs used the inverse foot trajectory. When four leg walk with a quadrant phase, the legged robot moved like a trot gait for the uneven velocity in a gait circle. The front legs have higher step than the back legs in this experiment.

As shown in Fig. 7, the current of back legs has lower offset than the front legs in the experiments, for their lower steps than front legs. The small amplitude fluctuations in the current curves were caused by the gravity center adjusting, which affects the feet’s contact force. The current range of four legs with the semicircle feet is lower than the rigid feet. Firstly, the

semicircle feet could reduce the maximum current of the front legs and have small effect on the minimum current of the front legs. In Fig. 7(a), maximum current values of front legs are larger than 8 A. However, the maximum current values are either between 8 A and 7 A, or even lower than 7 A in Fig. 7(b). Besides, the maximum current values are all nearly 6 A in Fig. 7(c). Secondly, the semicircle feet have small effect on the maximum current of the back legs, and can reduce the absolute values of the negative minimum value. In Fig. 7(a), the minimum current values of back legs are all nearly -4 A. However, the minimum current values are nearly -3 A in Fig. 7(b), and they are nearly -2.5 A in Fig. 7(c).

The experimental results show that, the quadruped robot with semicircle feet need lower driving torque in inner trigger configuration, and the lower stiffness semicircle has better effect than the higher stiffness ones.

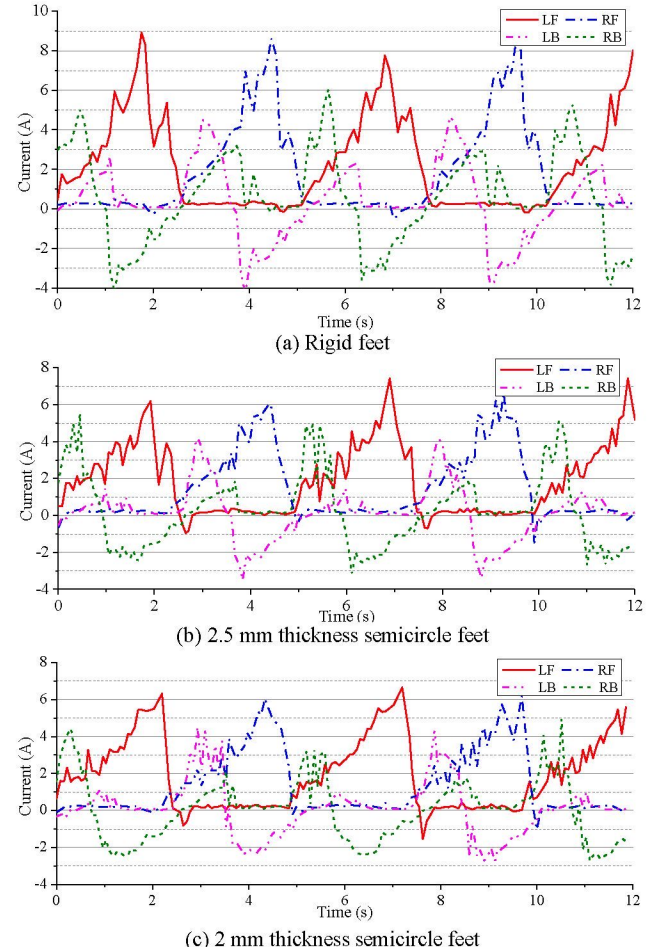


Fig. 7. The actual current of the four motors when robot walked with inner trigger configuration: (a) the results of robot with rigid feet; (b) the results of robot with 2.5 mm thickness semicircle feet; (c) the results of robot with 2 mm thickness semicircle feet

The relationships between the current and the crank angle were shown in Fig. 8, from which the gait phase could be obtained. As shown in Fig. 8(a) and 8(b), the crank angles of swing phase in the front legs are between 150 degrees and 315 degrees; in Fig. 8(c) and 8(d), the crank angles of swing phase in the back legs are between 240 degrees and 315 degrees.

There are small differences between semicircle feet and rigid feet, no matter the front legs or the back legs.

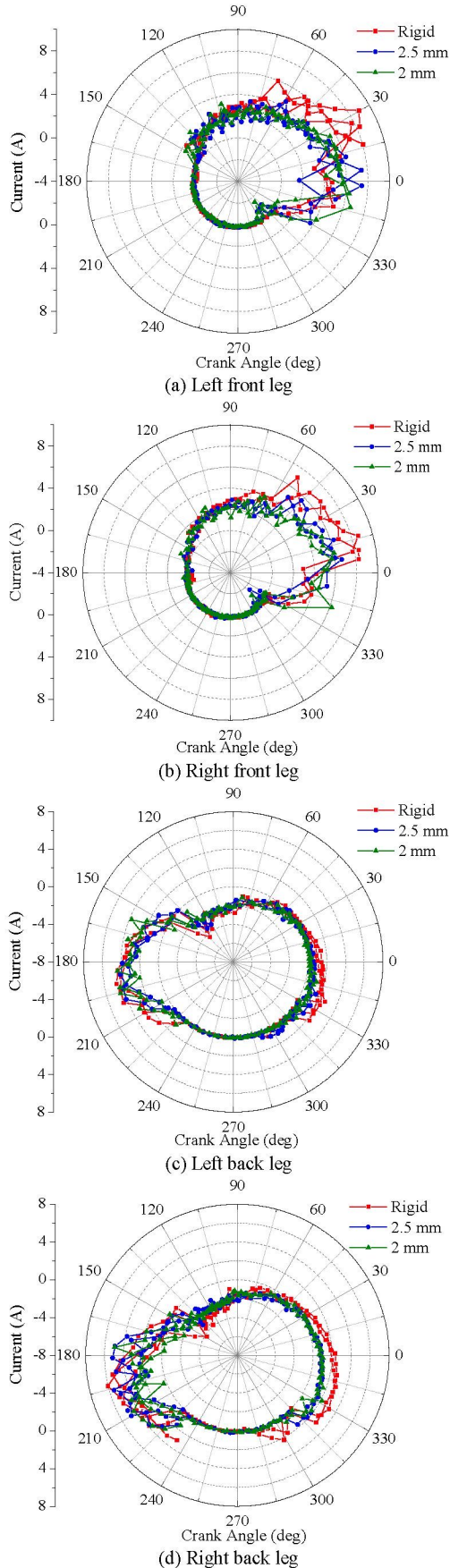


Fig. 8. The current curves in a crank cycle. In (a) and (b), the crank angle of the front legs is the same to the θ_1 in Fig.1. In (c) and (d), the crank angle of the back legs is a horizon opposite to θ_1 in Fig.1: the 0, 90, 180 and 270 degrees in (c) and (d) are the same to the 180, 90, 0, 270 degrees of θ_1 in Fig.1, respectively.

B. Robot in configuration that both elbow joints angled in parallel

The front and back legs moved with the same feet trajectory when robot was in parallel trigger configuration. In this experiment, the robot walked with a “LB-LF-RB-RF” walk gait, and had a quadrant phase difference. The back legs stand for the main gravity force for asymmetric mechanical structure.

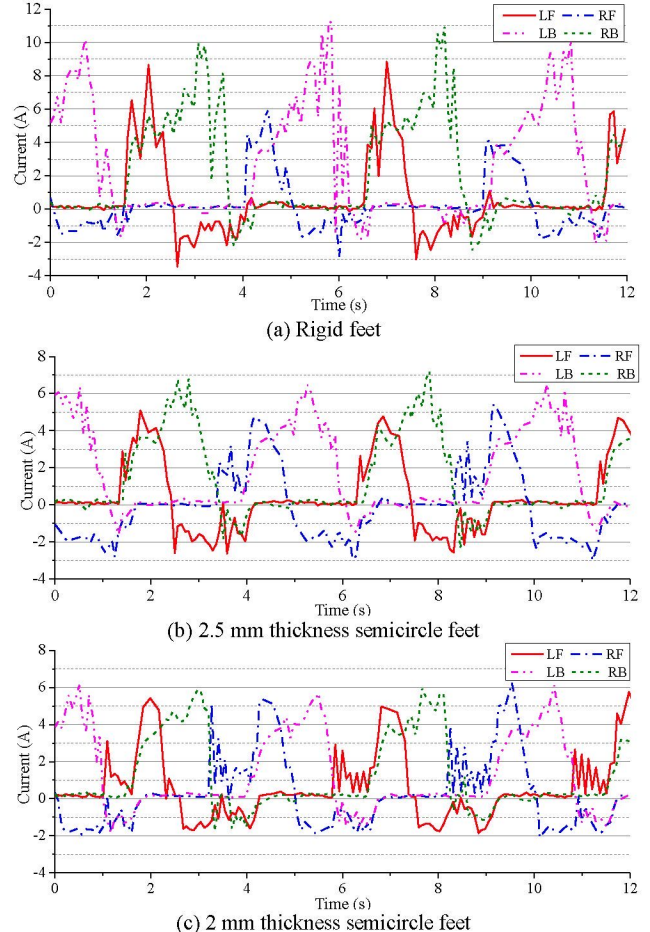


Fig. 9. The actual current of the four motors when robot walked with parallel trigger configuration: (a) the results of robot with rigid feet; (b) the results of robot with 2.5 mm thickness semicircle feet; (c) the results of robot with 2 mm thickness semicircle feet.

In Fig. 9, the current curves present a slightly gait. The current of the back legs has a higher offset than front legs and h. There are many small magnitude fluctuations in the curves for influence of the gravity adjusting. In this experiment, the semicircle feet mainly reduce the maximum current of the back legs and the negative minimum current of the front legs. As shown in Fig. 9(a), the maximum current of back legs is over the 10 A, and the minimum current of the back legs is below the -3 A. However, as shown in Fig. 9(b), the maximum current of the back legs is between 7 A and 6 A, the minimum

current of front legs is near -3 A. Besides, as shown in Fig. 9(c), the maximum current of the back legs is below 6 A, and the minimum current of the front legs is above -2 A.

Therefore, the semicircle could efficiently reduce the driving torque when robot walked in parallel configuration, and the lower stiffness ones behaved better than the high stiffness ones.

V. CONCLUSION AND FUTURE WORK

With a goal to reduce the driving torque of the multi-legged robot based on closed-chain mechanism, semicircle feet was designed as compliant feet and tested on a quadruped robot. Firstly, a special trajectory was achieved after a kinematic analysis and optimization of the six-bar closed-chain mechanism with one degree of freedom. Based on these analyses, a quadruped robot based on closed-chain mechanism was built and could be assembled to inner trigger and parallel trigger configurations. Then, two semicircle feet with thickness of 2 mm and 2.5 mm were designed, and their stiffness was 15.38 and 36.32 N/mm respectively. Finally, in order to observe semicircle feet's performance in closed-chain legged robot walking on the ground, two experiments of robot in inner trigger and parallel trigger configurations were carried out, and the motors current was measured to show the driving torque. The experimental results showed that the compliant feet could efficiently reduce the driving torque, especially in parallel configuration. Besides, the lower stiffness semicircle feet behaved better than the high stiffness ones in the two experiments. This primary investigation illustrated that the compliant feet could improve the locomotion performance of a quadruped robot based on closed-chain mechanism legs.

However, only qualitatively analysis about compliant feet's performance in reducing the driving torque was presented. To further clear that how the compliant feet's parameters affect the multi-legged robot based on closed-chain mechanism, the quantitative analysis will be taken in the future. The analysis goal is not only the driving torque, but also the forward speed, the pitch and rolls characteristics, stability and so on.

REFERENCES

- [1] M. P. Murphy, A. Saunders, C. Moreira, A. A. Rizzi, and M. Raibert, "The LittleDog robot," *International Journal of Robotics Research*, vol. 30, pp. 145-149, Feb 2011.
- [2] M. Zucker, N. Ratliff, M. Stolle, J. Chestnutt, J. A. Bagnell, C. G. Atkeson, et al., "Optimization and learning for rough terrain legged locomotion," *International Journal of Robotics Research*, vol. 30, pp. 175-191, 2011.
- [3] B. Klaassen, R. Linnemann, D. Spenneberg, and F. Kirchner, "Biomimetic walking robot SCORPION: Control and modeling," *Robotics and autonomous systems*, vol. 41, pp. 69-76, 2002.
- [4] S. Cordes, K. Berns, M. Eberl, W. Ilg, and P. Buhrlé, "On the design of a four-legged walking machine," in *8th International Conference on Advanced Robotics*, 1997, pp. 65-70.
- [5] W. Ilg, K. Berns, H. Jedele, J. Albiez, R. Dillmann, M. Fischer, et al., "BISAM: From small mammals to a four legged walking machine," in *Proceedings of the Fifth International Conference on Simulation of Adaptive Behaviour*, 1998, pp. 400-407.
- [6] R. Playter, M. Buchler, and M. Raibert, "BigDog" in *Proceedings of SPIE: Unmanned Systems Technology VIII*, 2006, pp. 62302O-1 - 62302O-6.
- [7] C. Semini, N. G. Tsagarakis, E. Guglielmino, and D. G. Caldwell, "Design and experimental evaluation of the hydraulically actuated prototype leg of the HyQ robot," in *2010 IEEE/RSJ International Conference on Intelligent Robots and Systems (IROS)*, Taipei, Taiwan, 2010, pp. 3640-3645.
- [8] T. Boaventura, C. Semini, J. Buchli, M. Frigerio, M. Focchi, and D. G. Caldwell, "Dynamic torque control of a hydraulic quadruped robot," in *2012 IEEE International Conference on Robotics and Automation (ICRA)*, 2012, pp. 1889-1894.
- [9] T. Jansen. *The Jansen's Strandbeest*. Available: <http://www.strandbeest.com/>
- [10] S. Floyd and M. Sitti, "Design and development of the lifting and propulsion mechanism for a biologically inspired water runner robot," *Robotics, IEEE Transactions on*, vol. 24, pp. 698-709, 2008.
- [11] H. S. Park, S. Floyd, and M. Sitti, "Roll and Pitch Motion Analysis of a Biologically Inspired Quadruped Water Runner Robot," *International Journal of Robotics Research*, vol. 29, pp. 1281-1297, Sep 2010.
- [12] Z. Wang, E. Dong, J. Hu, H. Wang, et al., "System Dynamics Simulation and Prototype Design of a High Efficient Legged Robot Based on Hybrid-Driven Mechanism", in *2013 International Conference on Advanced Intelligent Mechatronics (AIM)*, Wollongong, Australia, 2013, pp. 536-541
- [13] R. M. Alexander, "Elastic energy stores in running vertebrates," *American Zoologist*, vol. 24, pp. 85-94, 1984.
- [14] B. Brown and G. Zeglin, "The bow leg hopping robot," in *Robotics and Automation, Proceedings. 1998 IEEE International Conference on*, 1998, pp. 781-786.
- [15] C. Ordóñez, N. Gupta, E. Collins, J. Clark, and A. M. Johnson, "Power modeling of the XRL hexapedal robot and its application to energy efficient motion planning," in *Proceedings of the International Conference on Climbing and Walking Robots*, 2012.
- [16] G. C. Haynes, J. Pusey, R. Knopf, A. M. Johnson, and D. E. Koditschek, "Laboratory on legs: an architecture for adjustable morphology with legged robots," in *Proceedings of SPIE, Unmanned Systems Technology XIV*, 2012, pp. 83870W-1 - 83870W-14.